Supporting Information

Hydrogen-bond-induced quantum interference in single-molecule junctions of regioisomers

Lingbing Ge,[a#] Songjun Hou,[b#] Yaorong Chen,[c#] Qingqing Wu,[b] Lanxin Long,[a] Xingzhou Yang,[a] Yu Ji,[a] Luchun Lin,[c] Guodong Xue,[a] Junyang Liu,[c] Xiaodong Liu,*[a] Colin J. Lambert,*[b] Wenjing Hong,*[c] and Yonghao Zheng*[a]

[a]School of Optoelectronic Science and Engineering, University of Electronic Science and Technology of China (UESTC), Chengdu 610054, People's Republic of China.

[b]Department of Physics, Lancaster University, Lancaster LA1 4YB, UK.

[c]State Key Laboratory of Physical Chemistry of Solid Surfaces, College of Chemistry and Chemical Engineering, Xiamen University, Xiamen 361005, People's Republic of China.

*Corresponding author. Email: xdliu@uestc.edu.cn (X.L.); c.lambert@lancaster.ac.uk (C.L.); whong@xmu.edu.cn (W.H.); zhengyonghao@uestc.edu.cn (Y.Z.)

[#]These authors contributed equally to this work.

Table of Contents

Section S1. Synthesis and characterization of BIT-Zwitterion and BIT-Neutral

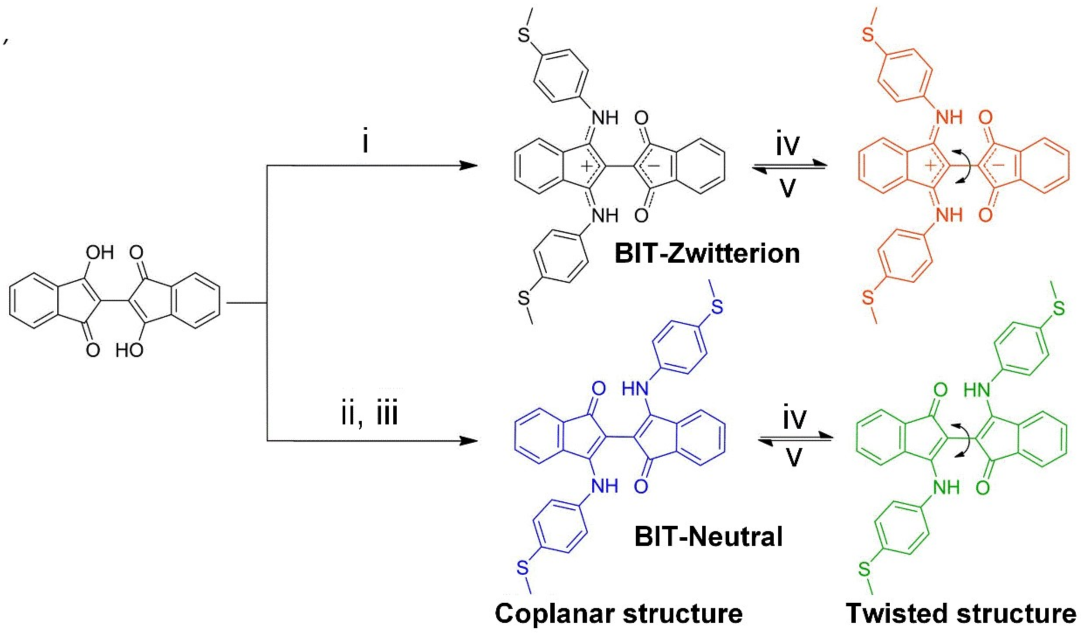

Scheme S1. The synthetic routes of target molecules **BIT-Zwitterion** and **BIT-Neutral**. Reagents and conditions: (i) 4-(Methylthio)aniline, acetic acid, mixture of *n*-butyl alcohol and *iso*-propyl alcohol, reflux; (ii) triethylamine, pyridine, benzenesulfonyl chloride, dichloromethane, 0 °C; (iii) 4-(Methylthio)aniline, room temperature; (iv) increase solvent polarity; (v) decrease solvent polarity.

Synthesis and characterization of BIT-OH$_2$

Material **BIT-OH$_2$** was prepared according to the literature procedures.[1] All reagents were purchased from Sigma-Aldrich, Acros and Adamas and used as received. Flash column chromatography was performed with Haiyang silica gel (200-300 mesh). All reaction mixtures and column eluents were monitored by TLC using commercial Huanghai glass plates (HSGF 254, 2.5 x 8 cm). The plates were visualized under UV radiation at 254 and 365 nm. UV-Vis-NIR absorption spectra were recorded with a UV-Vis spectrophotometer (Shimadzu, UV-2600). Nuclear magnetic resonance (NMR) spectra were obtained on a Bruker AV II-400 MHz spectrometer. High-resolution mass spectra (HRMS) were recorded on a Waters-Q-TOF-Premier (ESI) mass spectrometer. Cyclic voltammograms (50 mV s^{-1} scan rate) were carried out using a silver (Ag) wire as reference electrode and a platinum (Pt) wire as working electrode in dry DCM with

0.1 M $n\mathrm{Bu}_4\mathrm{NPF}_6$ as supporting electrolyte.

Synthesis of BIT-Zwitterion

BIT-OH$_2$ (0.29 g, 1.0 mmol) was added into a 100 ml round-bottom flask with a 50:50 (v/v) *n*-butanol/*iso*-propanol solvent mixture. Then, the above mixture was refluxed until all the starting materials were dissolved. 4-(Methylthio)aniline (0.42 g, 3.0 mmol) and acetic acid (0.18 g, 3.0 mmol) were slowly added. The reaction was allowed to reflux for 12 h and then cool down to room temperature. The dark solid was collected, washed with 50 ml of methanol and purified by column chromatography on silica gel (eluent: DCM), followed by recrystallization from DCM/methanol mixture. Yield: 41%. ^{1}H NMR (400 MHz, CD_2Cl_2): δ = 15.26 (2 H, s), 7.32-7.24 (12 H, m), 6.83 (2 H, s), 6.43 (2 H, s), 2.54 (6 H, s). ^{13}C NMR (100 MHz, $CDCl_3$): δ = 192.01, 162.34, 139.06, 138.08, 136.62, 135.69, 131.12, 130.15, 126.95, 125.65, 123.69, 118.59, 109.78, 100.10, 15.80. HRMS (ESI$^+$): calcd. for $C_{32}H_{24}N_2O_2S_2$ 532.1279, found $[M+H]^+$ 533.1323.

Synthesis of BIT-Neutral

BIT-OH$_2$ (0.20 g, 0.7 mmol) was suspended in a 250 ml round-bottom flask in 25 ml of dry DCM and 0.2 ml of triethylamine under a nitrogen atmosphere. The reaction mixture was cooled to 0 ºC in a salt ice bath. *p*-Toluenesulfonyl chloride (0.52 g, 2.7 mmol) was dissolved in 0.2 ml of DCM and 0.1 ml of pyridine in a separate flask. This solution was added dropwise into the reaction mixture which turned dark green. After stirring at 0 ºC for 10 min, 4-(methylthio)aniline (0.29 g, 2.1 mmol) was added. The reaction mixture was allowed to warm to room temperature for 6 h. The solvent was removed, and the crude product was purified by column chromatography on silica gel (20% EA in hexanes), followed by recrystallization from DCM/hexane. Yield: 29%. ^{1}H NMR (400 MHz, $CDCl_3$): δ = 11,69 (2 H, s), 7.32-7.16 (12 H, m), 7.00 (2 H, s), 6.44-6.43 (2 H, m), 2.53 (6 H, s). ^{13}C NMR（100 MHz, $CDCl_3$）: 193.48，161.00，137.49，137.20，136.37，136.11，131.20，130.08，127.06，125.39，122.55，120.14，106.90，16.05. HRMS(ESI$^+$): calcd. for $C_{32}H_{24}N_2O_2S_2$ 532.1279, found $[M+H]^+$ 533.1304.

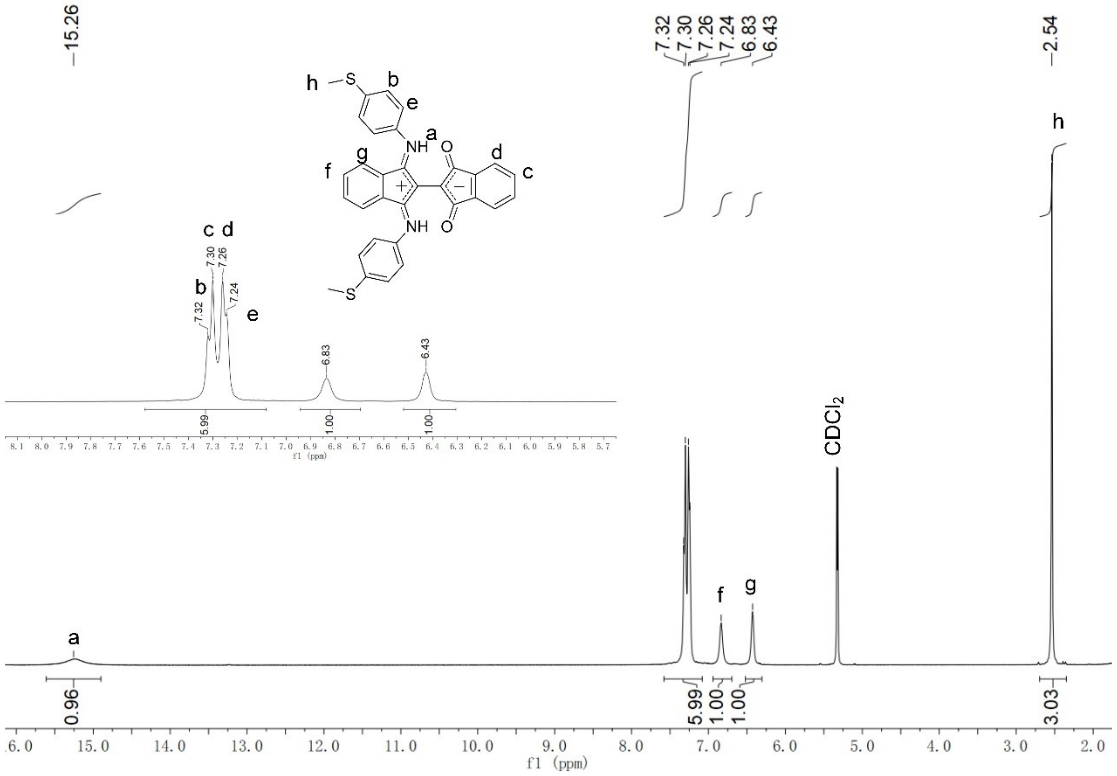
15.26
7.32
7.30
7.26
7.24
6.83
6.43
2.54
h
S
b
e
NH
a
f
g
d
c
O
O
+
−
NH
S
c d
7.30
7.26
b
7.32
7.24
e
6.83
6.43
5.99
1.00
1.00
8.1 8.0 7.9 7.8 7.7 7.6 7.5 7.4 7.3 7.2 7.1 7.0 6.9 6.8 6.7 6.6 6.5 6.4 6.3 6.2 6.1 6.0 5.9 5.8 5.7
f1 (ppm)
$CDCl_2$
f
g
a
0.96
5.99
1.00
1.00
3.03
16.0 15.0 14.0 13.0 12.0 11.0 10.0 9.0 8.0 7.0 6.0 5.0 4.0 3.0 2.0
f1 (ppm)

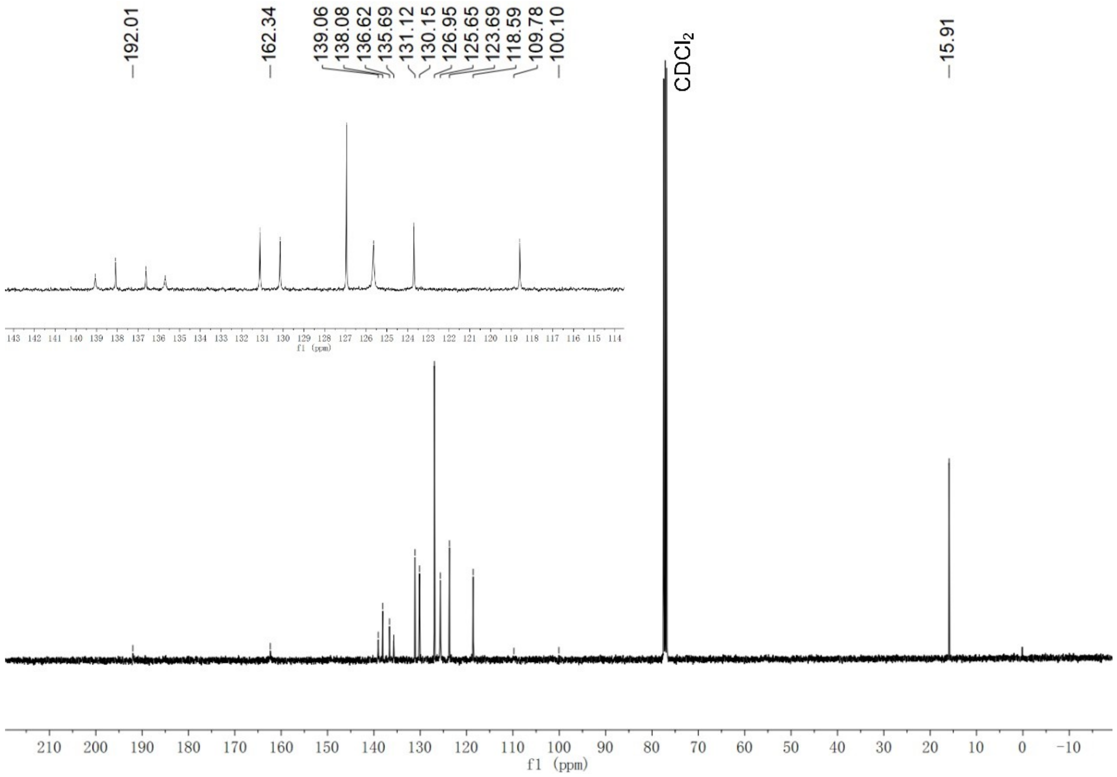
192.01
162.34
139.06
138.08
136.62
135.69
131.12
130.15
126.95
125.65
123.69
118.59
109.78
100.10
$CDCl_2$
15.91
143 142 141 140 139 138 137 136 135 134 133 132 131 130 129 128 127 126 125 124 123 122 121 120 119 118 117 116 115 114
f1 (ppm)
210 200 190 180 170 160 150 140 130 120 110 100 90 80 70 60 50 40 30 20 10 0 −10
f1 (ppm)

Figure S1. ^{1}H and ^{13}C NMR spectra of **BIT-Zwitterion**.

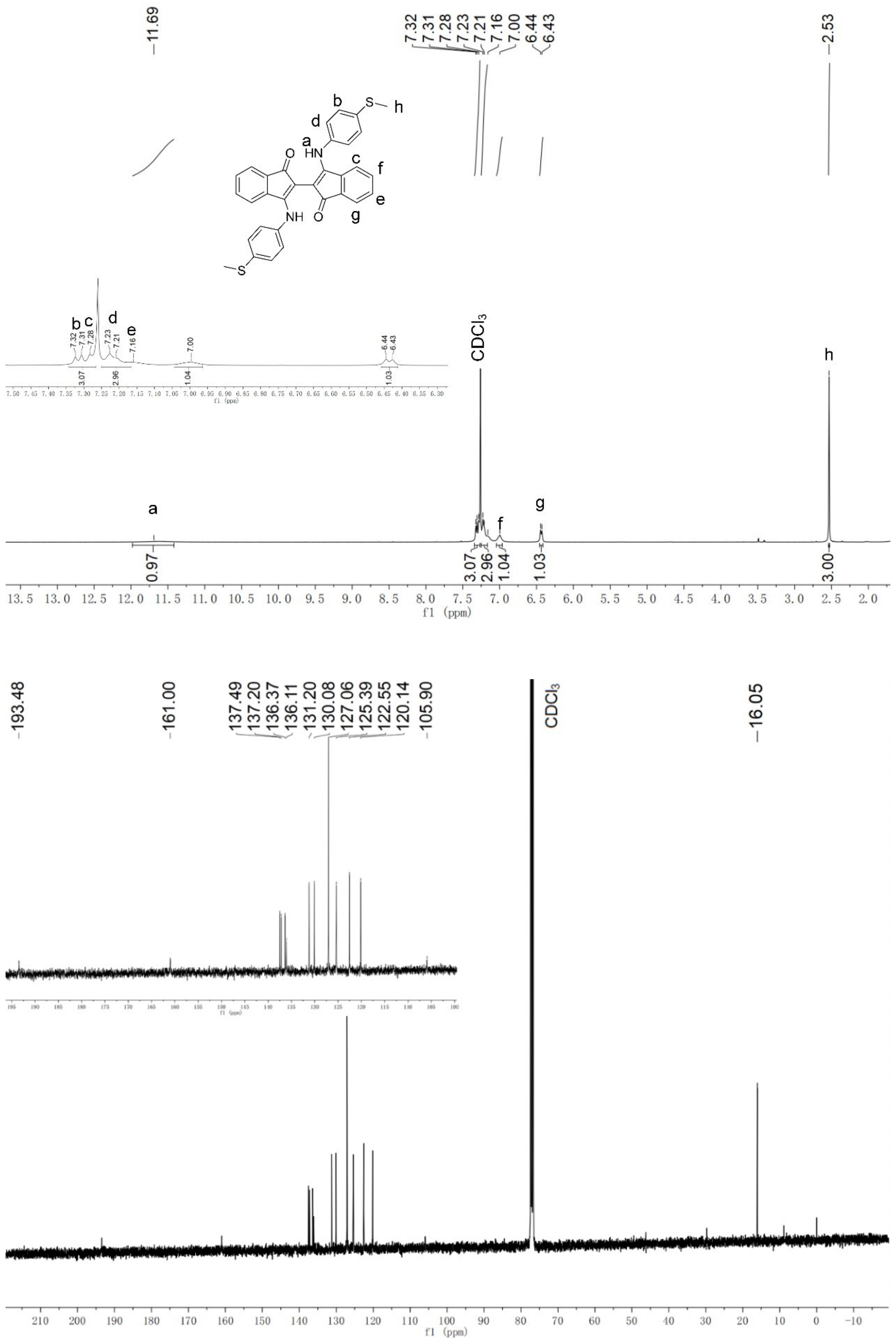

Figure S2. ^{1}H and ^{13}C NMR spectra of **BIT-Neutral**.

Section S2. UV-Vis absorption spectra

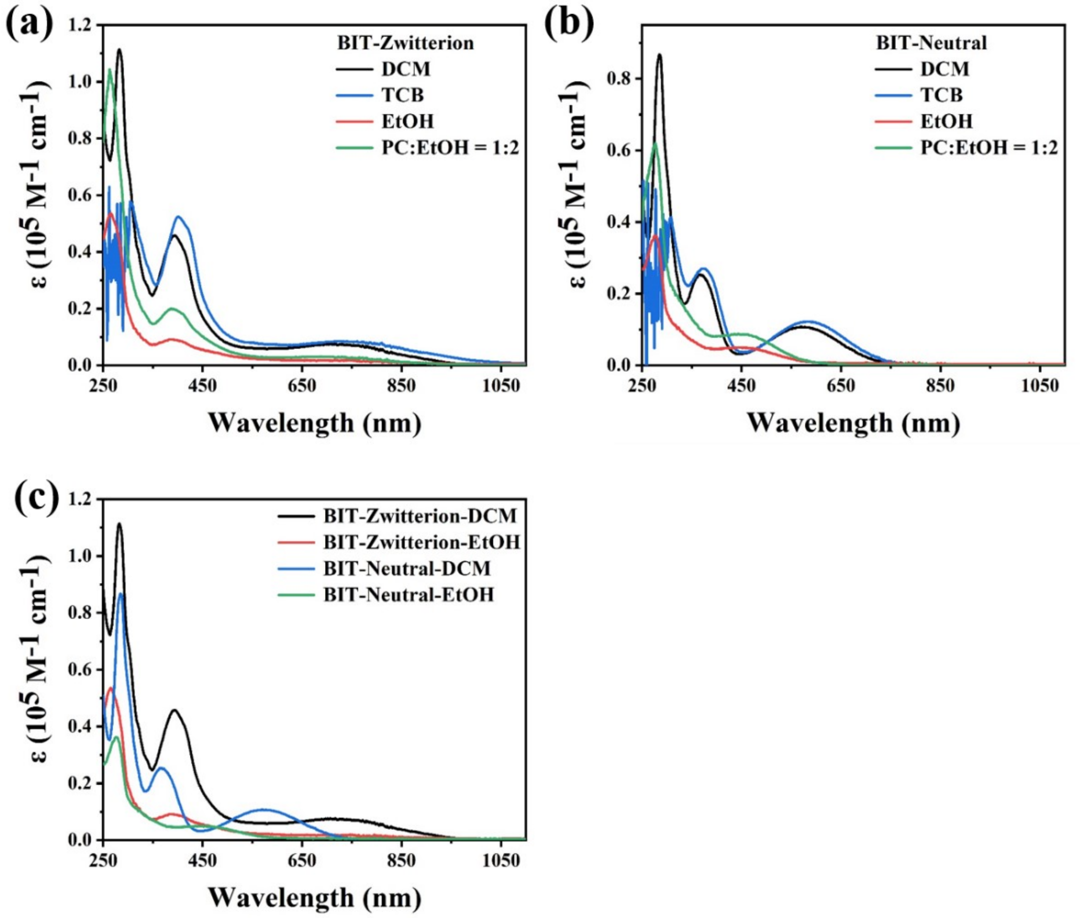

Figure S3. Absorption spectra of (a) **BIT-Zwitterion** and (b) **BIT-Neutral** in different solvents. Both isomers show similar changes in the absorption spectrum in DCM (TCB) and EtOH (PC:EtOH). (c) Absorption spectra of **BIT-Zwitterion** and **BIT-Neutral** in DCM and EtOH.

Table S1. Molar extinction coefficients at λ_{max} of **BIT-Zwitterion** and **BIT-Neutral** in different solvents.

Compound	**Solvent**	$\boldsymbol{\lambda_{max}^{1}}$ **(nm)**	$\boldsymbol{\varepsilon}$ **at** $\boldsymbol{\lambda_{max}^{1}}$ **(10^5 M^{-1} cm^{-1})**	$\boldsymbol{\lambda_{max}^{2}}$ **(nm)**	$\boldsymbol{\varepsilon}$ **at** $\boldsymbol{\lambda_{max}^{2}}$ **(10^5 M^{-1} cm^{-1})**	$\boldsymbol{\lambda_{max}^{3}}$ **(nm)**	$\boldsymbol{\varepsilon}$ **at** $\boldsymbol{\lambda_{max}^{3}}$ **(10^5 M^{-1} cm^{-1})**
BIT-Zwitterion	DCM	282	1.11	394	0.46	717	0.08
	TCB	306	0.58	401	0.52	733	0.09
	EtOH	265	0.54	387	0.09	746	0.02
	PC:EtOH	263	1.04	387	0.20	735	0.03
BIT-Neutral	DCM	286	0.87	367	0.25	570	0.11
	TCB	308	0.41	373	0.27	584	0.12
	EtOH	277	0.36	450	0.05	-	-
	PC:EtOH	277	0.62	443	0.09	-	-

Section S3. Cyclic voltammetry

Cyclic voltammetry (CV) measurements were carried out in DCM solution with tetrabutylammonium hexafluorophosphate (0.1 M) as supporting electrolyte at a scan rate of 50 mV s^{-1}. Pt wire, glassy carbon and saturated calomel electrode (SCE) were used as counter electrode, working electrode and reference electrode, respectively. The cyclic voltammograms of **BIT-Zwitterion** and **BIT-Neutral** show similar two reversible oxidation waves, and half-wave potentials $E_{1/2}$ were calculated and marked with red stars (Figure S4a). The HOMO energy levels of both compounds were estimated from the first half-wave potential in Figure S4a using ferrocene (Fc/Fc^+) as reference (Figure S4b). The equations used to calculate the energy levels are: $E_{HOMO} = -(E^{ox}_{1/2} - E^{ox}_{Fc/Fc^+} + 4.8)$; $E_{LUMO} = E_{HOMO} + E_g$, where E_g represents optical band gap, calculated from the onset of absorption ($E_g = 1240/\lambda_{onset}$).[2,3]

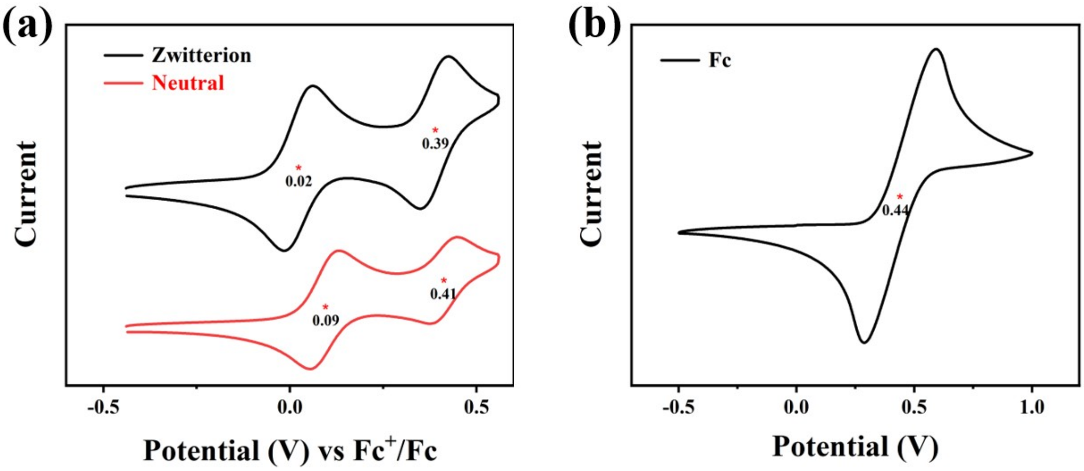

Figure S4. (a) Cyclic voltammograms of **BIT-Zwitterion** and **BIT-Neutral** in dry DCM vs Fc/Fc^+. (b) Cyclic voltammogram of ferrocene in dry DCM.

Section S4. X-ray crystallography

Purple single crystal of **BIT-Neutral** with coplanar configuration was grown by slow evaporation of DCM/hexane. Dark-red single crystal of **BIT-Neutral** with twisted configuration was obtained after slow evaporation of DCM/methanol. CCDC (**BIT-Neutral** (coplanar): 1963994 and **BIT-Neutral** (twisted): 1991442).

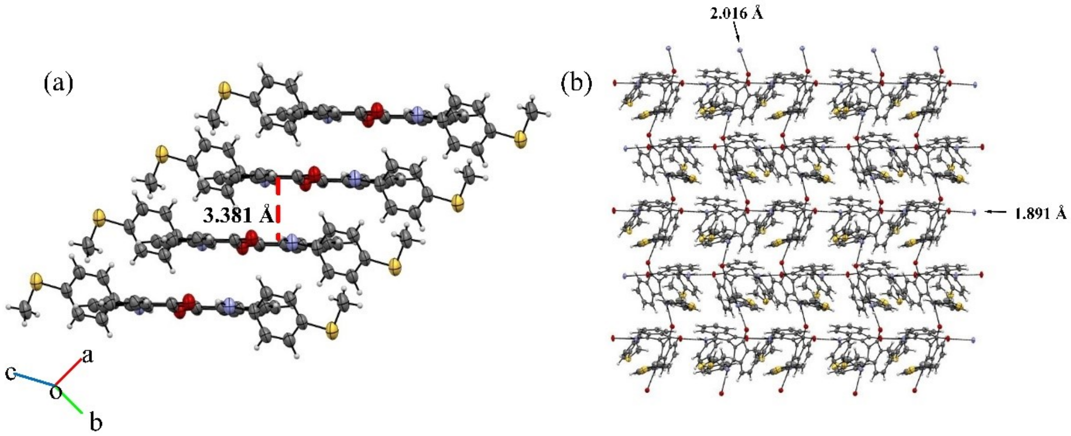

Figure S5. Crystallographic views of **BIT-Neutral**. (a) Selected packing view of coplanar configuration (red dashed line represents the interplanar distance). (b) Selected packing view of twisted configuration (black line represents the exmaple of intermolecular hydrogen bonding).

Section S5. Computational details

EPS calculations were performed with Gaussian 16 program suite.[4] The B3LYP functional and 6-31g(d) basis set were used. The maps of isosurface plot of ESP are shown in Figure S6. The maps were illustrated using Multiwfn and VMD.[5]

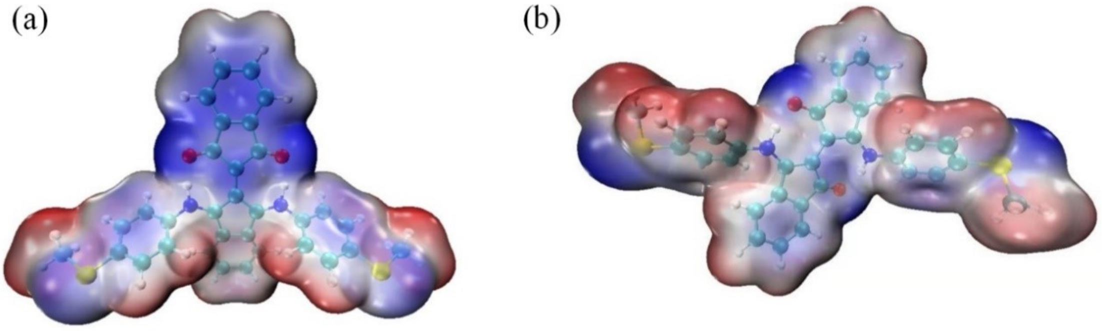

Figure S6. The ESP color maps of (a) **BIT-Zwitterion** and (b) **BIT-Neutral**.

Section S6. Measurement (STM-BJ)

We employed the home-built scanning tunneling microscope-break junction (STM-BJ) setup to measure the single-molecule conductance. A gold wire (99.9% in purity, 0.25 mm diameter, Jiaming, Beijing) was burned by butane flame into a bead and then fixed as the STM tip. The gold-plated silicon wafers that were used as the substrates were pretreated by piranha lotion (98% H_2SO_4: 30% H_2O_2 = 3:1, v/v) followed by washing with ultra-pure water (18.2 MΩ·cm, Milli-Q system) before each experiment, and then fastened. During the measurements, the movement of the tip was driven by a combination of a piezo stack and a stepper motor, and controlled by the feedback current between the two electrodes to construct repeated nanogap. After dropping 5 μl target solution onto the substrate, a single-molecule was trapped at the periodic break junction to form single-molecule junction. According to the applied bias voltage between the tip and substrate, the real-time conductance of junction was detected by I-V converter with a sampling rate of 20 kHz. The construction of 1D or 2D conductance and relative displacement histogram can refer to our recent works.[6,7]

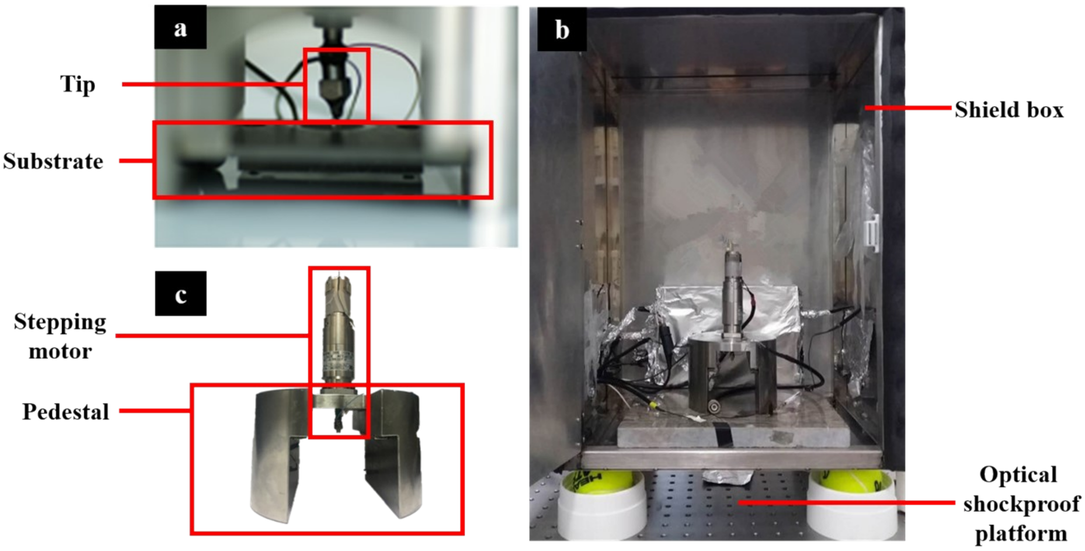

Figure S7. Schematic diagram of home-built STM equipment.

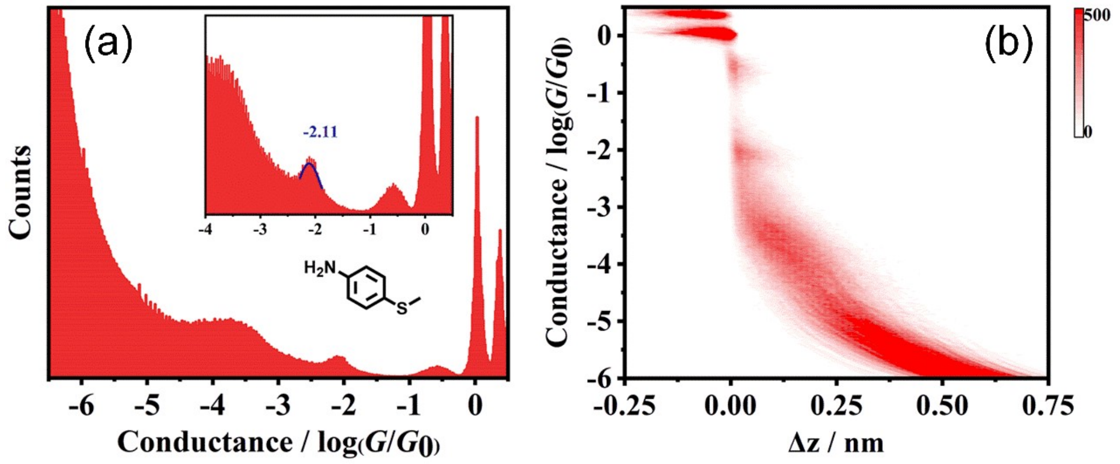

Figure S8. (a) 1D conductance histogram of mercaptoaminobenzene. The inset shows the magnified view with Gaussian fitting. (b) 2D conductance-displacement histogram of mercaptoaminobenzene.

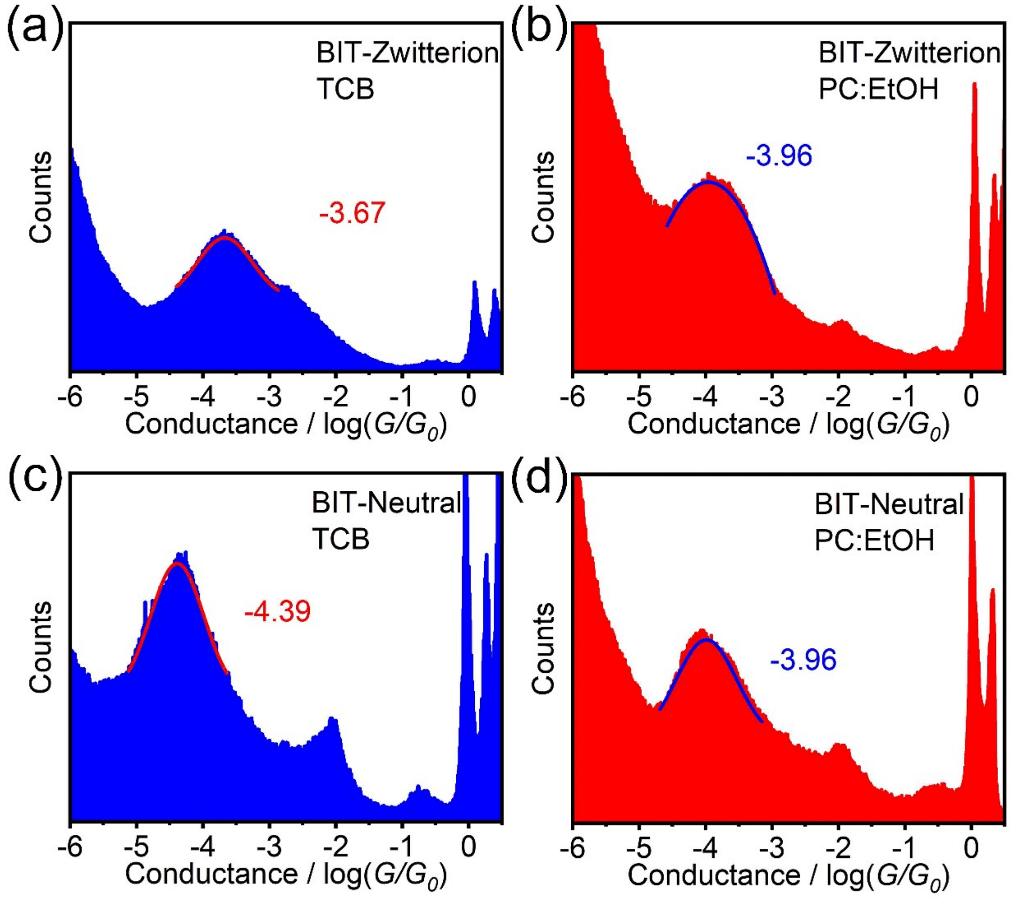

Figure S9. 1D conductance histograms of (a, b) **BIT-Zwitterion** and (c, d) **BIT-Neutral** in (a, c) TCB and (b, d) PC:EtOH solutions with Gaussian fitting.

Section S7. DFT and transport calculations

Geometrical optimizations have been performed by using the DFT code SIESTA,[8] with a local density approximation LDA functional, a double-ζ polarized basis, a cutoff energy of 200 Ry and a 0.02 eV/Å force tolerance. To compute their electrical conductance, the molecules were each placed between two Au electrodes. For each structure, the transmission coefficient T(E) describing the propagation of electrons of energy E from the left to the right electrodes was calculated using Gollum code,[9] which combines the mean-field Hamiltonian and overlap matrices of the DFT code SIESTA with Landauer-based quantum transport theory using the expression

$$T(E) = Tr\left[\Gamma_L(E) G_r(E) \Gamma_R(E) G_r^{\dagger}(E)\right]$$

where $\Gamma_{L,R}(E) = i(\Sigma_{L,R}(E) - \Sigma_{L,R}{}^{\dagger}(E))/2$. $G_r(E) = \left(g^{-1} - \Sigma_L - \Sigma_R\right)^{-1}$. g is the Green's function of the isolated molecule. $\Gamma_{L,R}$ determines the widths of transmission resonances, $\Sigma_{L,R}(E)$ are the self-energies describing the contact between the molecule and left (L) and right (R) electrodes. While G_r is the retarded Green's function of the molecule in the presence of the electrodes.

To calculate the binding energy using SIESTA we use a counterpoise method to correct for basis set superposition errors that are inherent with the localized orbital basis sets that are employed. The binding energy between the **BIT-Zwitterion** and two ethanol molecules as shown in Figure S10. Here, the molecule **BIT-Zwitterion** is defined as entity A and two ethanol molecules as entity B. The ground state energy of the total system was calculated using SIESTA and is denoted E^{AB}_{AB}, with the DFT parameters defined previously. The energy of each entity was then calculated in a fixed basis, which was achieved using ghost atoms. Hence, the energy of the molecule **BIT-Zwitterion** in the presence of the fixed basis is defined as E^{AB}_{A} and for the two ethanol molecules as E^{AB}_{B}. The binding energy was then calculated using the following equation: binding energy = $E^{AB}_{AB} - E^{AB}_{A} - E^{AB}_{B}$. The binding energy between the **BIT-Zwitterion** and two ethanol molecules was then calculated as a function of rotation angle between the pendant group and the backbone of **BIT-Zwitterion**. The Voronoi charges are extracted based on SIESTA calculations.[8]

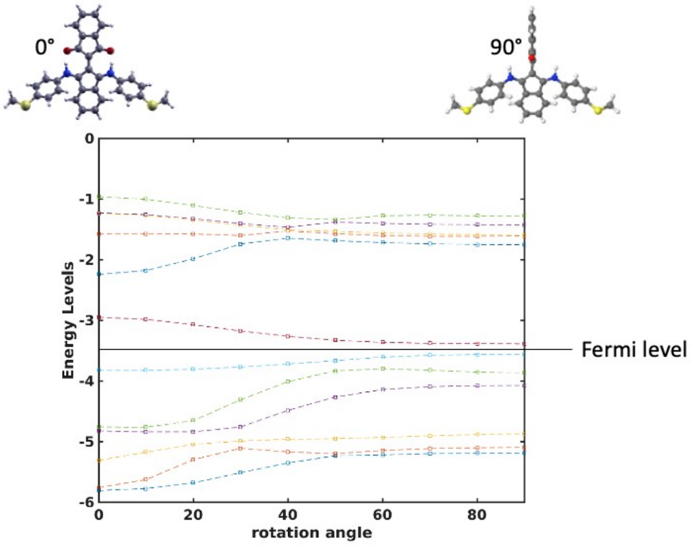

Figure S10. The energy levels evolve as the twisting the pendant group relative to the backbone of **BIT-Zwitterion**.

Section S8. Perturbation theory of protic solvent on the BIT-Zwitterion

When the protic solvents molecules are bonded to the molecules via hydrogen bond, the effect of the protic solvents could be treated as weak perturbation. Assuming the unperturbed system has a Hamiltonian H with a series of eigenvalues E^{n} and eigenstates ψ^{n}. With perturbation, the Hamiltonian becomes $H + H^{'}$ where $H^{'}$ is a very small Hamiltonian caused by the gating effect of solvent molecules. The new eigenvalues are evaluated via formula with only the first order perturbation is included.

$$E_{new}^{n} = E^{n} + \langle \psi^{n} \left| H^{'} \right| \psi^{n} \rangle \qquad (1)$$

Since HOMO and LUMO are most relevant to the molecules' transport property which could be measured in our MBJ experiment, only the changes of HOMO and LUMO after perturbation are investigated here. See Figure S11, in the case of BIT-Zwitterion. Two cases could be considered. One is the pendant group which is perturbed by protic solvent. Then $H^{'} = \begin{pmatrix} -r & 0 \\ 0 & 0 \end{pmatrix}$, where r is the perturbation on site 1 caused by solvent. Substituting H' to $Eq. (1)$, $E_{new}^{H} = E^{H} - \frac{r}{2}$, $E_{new}^{L} = E^{L} + 0$. Therefore, the HOMO-LUMO gap is increased by $\frac{r}{2}$. Second, if the backbone is perturbed by the solvent, $H^{'} = \begin{pmatrix} 0 & 0 \\ 0 & r \end{pmatrix}$, where r is the perturbation on site 2 caused by solvent. Then $E_{new}^{H} = E^{H} + \frac{r}{2}$, $E_{new}^{L} = E^{L} + r$, where H, L represent HOMO, LUMO respectively. the HOMO-LUMO gap is also increased by $\frac{r}{2}$.

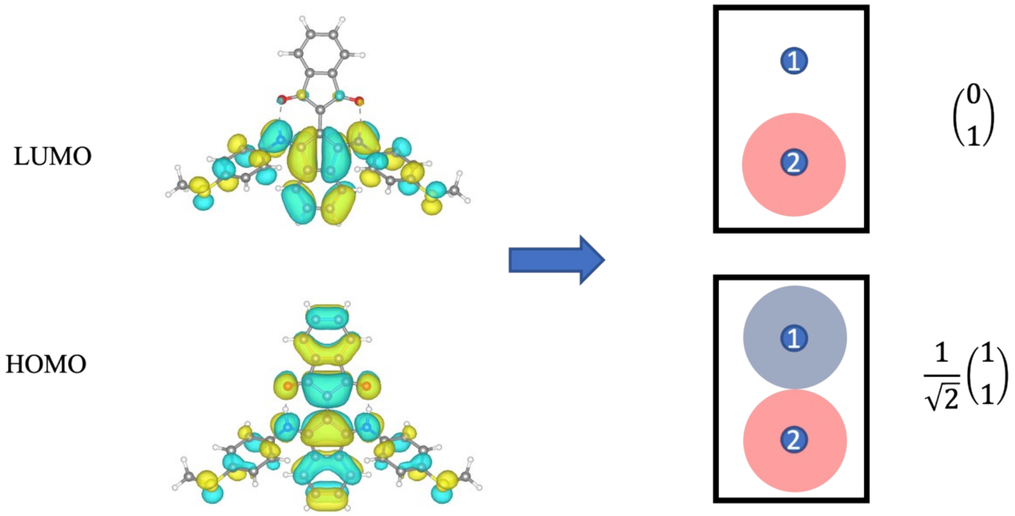

Figure S11. In the case of **BIT-Zwitterion**, the pendant and the backbone parts could be simplified to two sites. Then the HOMO and LUMO could be simplified to $\begin{pmatrix}0\\1\end{pmatrix}$ and $\frac{1}{\sqrt{2}}\begin{pmatrix}1\\1\end{pmatrix}$ respectively. The orbitals are represented by the large red and blue circles.

Table S2. In the case of **BIT-Zwitterion** with a twisted angle ~30°**,** evolutions of the HOMO and LUMO as the number of the ethanol surrounded increases. Three types of hydrogen bonds are considered, namely, the hydrogen of the hydroxyl points towards the oxygen of the pendant group, the oxygen of the hydroxyl points towards the nitrogen of the backbone and a mixture of them. In the following table, the first column means the number of ethanol molecules added. All the geometries are labeled from 1 to 10 as shown in second column are plotted in Figure S13.

Unit: eV		HOMO	LUMO	HL gap
Positive gating induced by the hydrogen bond between the proton of the ethanol and the oxygen of the backbone				
No Ethanol	1	-3.80	-3.32	0.48
1 ethanol	2	-4.03	-3.42	0.60
2 ethanol[a]	3	-4.17	-3.41	0.76
2 ethanol[b]	4	-4.22	-3.53	0.69
4 ethanol	5	-4.39	-3.44	0.95
Negative gating induced by the hydrogen bond between the oxygen of the ethanol and the nitrogen of the backbone				
1 ethanol	6	-3.93	-3.28	0.65
2 ethanol[a]	7	-3.95	-3.21	0.74
2 ethanol[b]	8	-4.09	-3.31	0.77
A mixture of positive gating and negative gating				
3 ethanol	9	-4.15	-3.35	0.8
4 ethanol	10	-4.13	-3.32	0.82

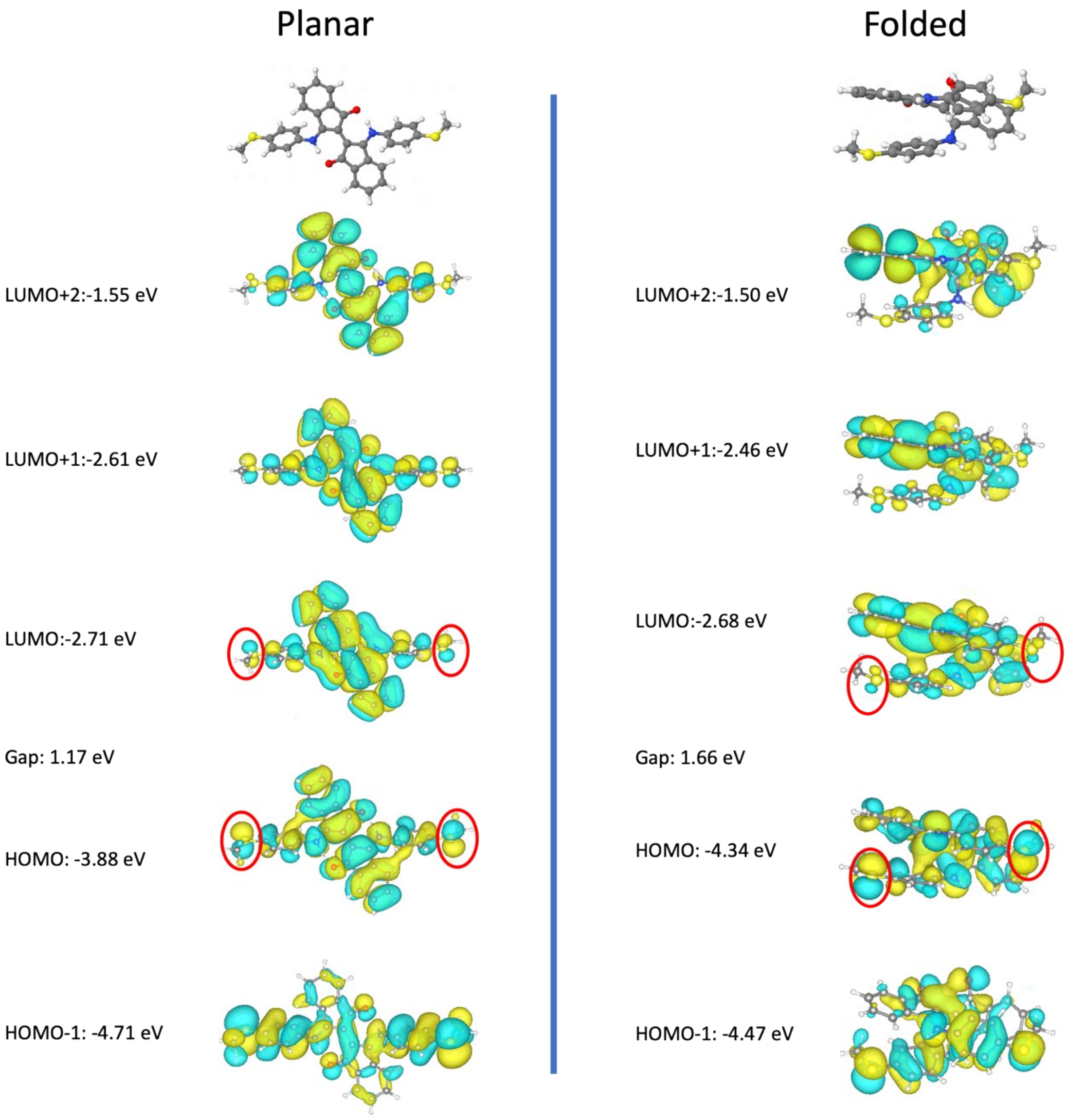

Figure S12. The frontier orbitals for planar and folded **BIT-Neutral** from HOMO-1 to LUMO+2. To predict quantum interference, the symmetries of HOMO and LUMO at two ends which are connected to two electrodes are indicated by the red circles.

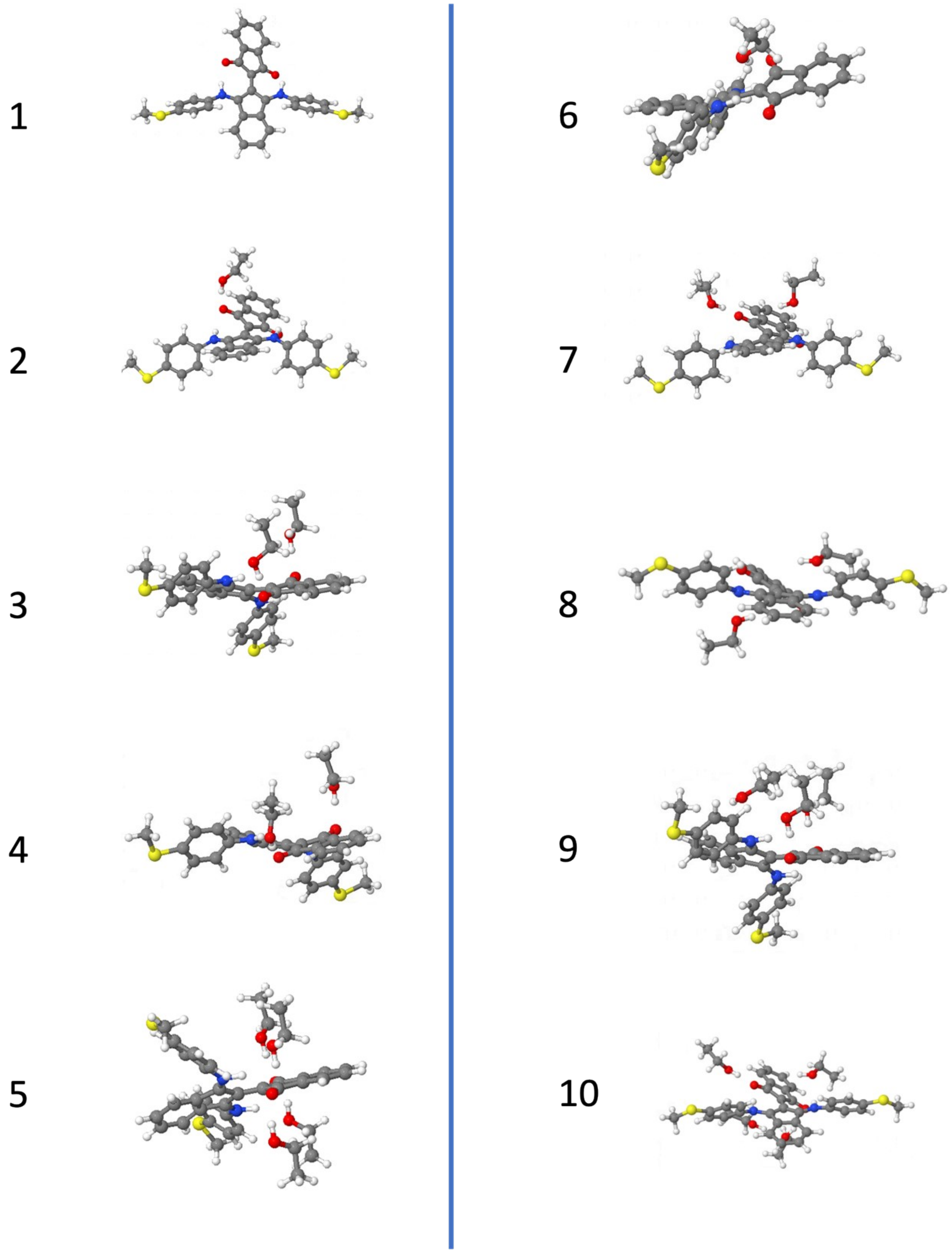

Figure S13. The geometries correspond to Table S2.

Section S9. Supplemental references

1 Dou, L.; Zheng, Y.; Shen, X.; Wu, G.; Fields, K.; Hsu, W. C.; Zhou, H.; Yang, Y.; Wudl, F. (2014) Single-Crystal Linear Polymers through Visible Light-Triggered Topochemical Quantitative Polymerization. Science. 343, 272-277.

2 Hu, X.; Chen, H.; Zhao, L.; Miao, M.; Han, J.; Wang, J.; Guo, J.; Hu, Y.; Zheng, Y. (2019) Nitrogen analogues of Chichibabin's and Müller's hydrocarbons with small singlet–triplet energy gaps. Chem. Commun. 55, 7812.

3 Xue, G.; Hu, X.; Chen, H.; Ge, L.; Wang, W.; Xiong, J.; Miao, F.; Zheng, Y. (2020) Understanding the nature of quinoidal and zwitterionic states in carbazole-based diradicals. Chem. Commun. 56, 5143.

4 Frisch, M. J.; Trucks, G. W.; Schlegel, H. B.; Scuseria, G. E.; Robb, M. A.; Cheeseman, J. R.; Scalmani, G.; Barone, V.; Petersson, G. A.; Nakatsuji, H.; Li, X.; Caricato, M.; Marenich, A. V.; Bloino, J.; Janesko, B. G.; Gomperts, R.; Mennucci, B.; Hratchian, H. P.; Ortiz, J. V.; Izmaylov, A. F.; Sonnenberg, J. L.; Williams-Young, D.; Ding, F.; Lipparini, F.; Egidi, F.; Goings, J.; Peng, B.; Petrone, A.; Henderson, T.; Ranasinghe, D.; Zakrzewski, V. G.; Gao, J.; Rega, N.; Zheng, G.; Liang, W.; Hada, M.; Ehara, M.; Toyota, K.; Fukuda, R.; Hasegawa, J.; Ishida, M.; Nakajima, T.; Honda, Y.; Kitao, O.; Nakai, H.; Vreven, T.; Throssell, K.; Montgomery, J. A., Jr.; Peralta, J. E.; Ogliaro, F.; Bearpark, M. J.; Heyd, J. J.; Brothers, E. N.; Kudin, K. N.; Staroverov, V. N.; Keith, T. A.; Kobayashi, R.; Normand, J.; Raghavachari, K.; Rendell, A. P.; Burant, J. C.; Iyengar, S. S.; Tomasi, J.; Cossi, M.; Millam, J. M.; Klene, M.; Adamo, C.; Cammi, R.; Ochterski, J. W.; Martin, R. L.; Morokuma, K.; Farkas, O.; Foresman, J. B.; Fox, D. J. (2016) Gaussian 16, Revision A.03; Gaussian Inc.: Wallingford, CT.

5 Lu, T.; Chen, F. Multiwfn: A Multifunctional Wavefunction Analyzer. (2012) J. Comput. Chem. 33, 580-592.

6 Bai, J.; Daaoub, A.; Sangtarash, S.; Li, X.; Tang, Y.; Zou, Q.; Sadeghi, H.; Liu, S.; Huang, X.; Tan, Z.; Liu, J.; Yang, Y.; Shi, J.; Meszaros, G.; Chen, W.; Lambert, C.; Hong, W. (2019) Anti-Resonance Features of Destructive Quantum Interference in Single-Molecule Thiophene Junctions Achieved by Electrochemical Gating. Nat. Mater. 18, 364-369.

7 Liu, J.; Zhao, X.; Zheng, J.; Huang, X.; Tang, Y.; Wang, F.; Li, R.; Pi, J.; Huang, C.; Wang, L.; Yang, Y.; Shi, J.; Mao, B.-W.; Tian, Z.-Q.; Bryce, M. R.; Hong, W. (2019) Transition from Tunneling Leakage Current to Molecular Tunneling in Single-Molecule Junctions. Chem. 5, 390-401.

8 Soler, J. e. M.; Artacho, E.; Gale, J. D.; Garc´ıa, A.; Junquera, J.; Ordej´on, P.; S´anchez-Portal, D. (2002) The SIESTA Method for Ab Initio Order-N Materials Simulation. J. Phys.: Condens. Matter. 14, 2745-2779.

9 Ferrer, J.; Lambert, C. J.; García-Suárez, V. M.; Manrique, D. Z.; Visontai, D.; Oroszlany, L.; Rodríguez-Ferradás, R.; Grace, I.; Bailey, S. W. D.; Gillemot, K.; Sadeghi, H.; Algharagholy, L. A. (2014) Gollum: A Next-Generation Simulation Tool for Electron, Thermal and Spin Transport. New J. Phys. 16, 093029.